Journal of Colloid and Interface Science 724 (2026) 141238

Contents lists available at ScienceDirect

Journal of Colloid And Interface Science

journal homepage: www.elsevier.com/locate/jcis

The impact of architecture and block lengths of poly(trimethylene carbonate-*b*-sarcosine) copolymers on their self-assembly behavior

Aljaž Pogorelec [a,b], Urška Češarek [a], Blaž Zdovc [a], Ema Žagar [a], David Pahovnik [a,*]

[a] Department of Polymer Chemistry and Technology, National Institute of Chemistry, Hajdrihova 19, Ljubljana SI-1000, Slovenia
[b] Faculty of Chemistry and Chemical Technology, University of Ljubljana, Večna pot 113, Ljubljana SI-1000, Slovenia

GRAPHICAL ABSTRACT

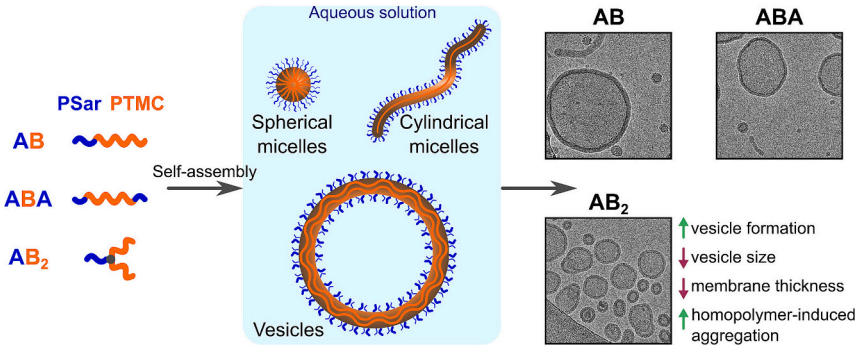

ARTICLE INFO

Keywords:
Amphiphilic block copolymers
Macromolecular architecture
Self-assembly
Polymersome membranes

ABSTRACT

The chemical composition and macromolecular architecture of amphiphilic block copolymers govern their self-assembly behavior in aqueous solution. Although a wide range of block chemistries and polymer architectures has been investigated, the influence of architecture on key properties of self-assembled structures, including polymersome membrane thickness, remains insufficiently understood. The increasing availability of well-defined block copolymers with diverse architectures provides an opportunity to systematically evaluate architectural effects by direct comparison with linear analogues of comparable composition. In this study, poly(trimethylene carbonate-*b*-sarcosine) (P(TMC-*b*-Sar)) copolymers with AB linear diblock, ABA linear triblock, and AB_2 miktoarm star architectures were synthesized by ring-opening polymerization, and their self-assembly in aqueous solution was characterized using electron microscopy and light scattering techniques. Copolymer architecture was found to significantly influence the morphology and size distribution of the resulting self-assembled structures. In particular, AB_2 miktoarm star copolymers formed polymersomes over a broader range of hydrophilic PSar weight fractions and hydrophobic PTMC block lengths than their AB linear counterparts. Furthermore, AB_2-derived polymersomes were more abundant in the smaller size range and exhibited measurably thinner membranes than AB-derived polymersomes with similar PTMC block lengths. We also demonstrate that residual PTMC homopolymer impurities generated during synthesis of certain AB_2 copolymers substantially alter vesicle morphology by promoting the aggregation of smaller vesicles. These findings demonstrate that both block copolymer architecture and the controlled presence of homopolymer impurities play important roles in

* Corresponding author.
E-mail address: david.pahovnik@ki.si (D. Pahovnik).

https://doi.org/10.1016/j.jcis.2026.141238
Received 25 May 2026; Received in revised form 17 July 2026; Accepted 27 July 2026
Available online 29 July 2026

governing block copolymer self-assembly and should be carefully considered in the design of polymersome-forming materials.

1. Introduction

Block copolymers are well known for their distinct self-assembly behavior in both the bulk phase and in solution [1–3]. Amphiphilic block copolymers have been extensively studied for their ability to form various supramolecular structures in aqueous solutions, most commonly micelles and vesicles [4–6]. The latter, also known as polymersomes, have been a major focus of applied research. Notably, polymersomes serve as nanocarriers for drug delivery, where they can outperform liposomes due to greater membrane stability and chemical versatility [7,8]. Furthermore, stimuli-responsive polymersomes allow for more accurate control of cargo release [9,10]. To better mimic complex biological systems such as cells and organelles, polymersomes are often modified with biological molecules [11]. Examples include attachment of ligands to the surface [12,13], incorporation of channel proteins into the membrane [14–16], and encapsulation of enzymes [15–17].

The self-assembly of amphiphilic block copolymers in aqueous solutions is thermodynamically driven by stretching of the hydrophobic blocks, hydrophobic block/water interfacial tension, and repulsive interactions between hydrophilic blocks [2,5,18]. These parameters are closely related to the geometry of the block copolymer, which can be described by the packing parameter ($p = v/a_0 l_c$), where v is the volume of the hydrophobic block, l_c is the length of the hydrophobic chains, and a_0 is the interfacial area between a single hydrophobic and hydrophilic chain [4–6,19]. In general, the value of p increases with the weight fraction and molecular weight of the hydrophobic block [20], and is associated with the interfacial curvature between the blocks. From higher to lower curvature, spherical micelles ($p < 0.33$), cylindrical micelles ($0.33 < p < 0.5$), and vesicles ($0.5 < p < 1$) are most likely to form [3–7]. Many other morphologies have been observed, including large compound micelles [21,22], multicompartment micelles [23], multicompartment vesicles [21,24], and lamellae [22]. This significant variability of self-assembled structures is influenced by factors such as the molecular weight dispersity of block copolymers and the kinetics during the self-assembly process [2,5–8].

Block copolymer architecture can also affect self-assembly behavior. Researchers have mainly focused on micellar structures, studying the critical micelle concentration, aggregation number, and hydrodynamic radius (R_h) as functions of copolymer architecture [25–28]. In addition, a theoretical study by Zhulina and Borisov [29] indicates that miktoarm stars are increasingly likely to self-assemble into polymersomes as the number of insoluble arms increases, which has also been observed experimentally. For example, Yin et al. [18] found that AB_2 miktoarm stars of poly(ethylene oxide) (PEO) and poly(L-lactic acid) could form vesicles over a much broader range of PEO volume fractions ($0.2 < f_{PEO} < 0.7$) compared to their AB linear diblock analogues ($0.2 < f_{PEO} < 0.4$). Similarly, Wang et al. [30] showed that AB_2 architecture could promote morphological transitions to structures with lower interfacial curvature than the corresponding AB analogue in the polymerization-induced self-assembly of copolymers containing PEO and poly(diacetone acrylamide) blocks. In a more recent study, Ozawa et al. [31] prepared copolymers with different architectures, using maltopentaose or cycloamylose as the hydrophilic block and poly(propylene oxide) (PPO) as the hydrophobic block. They observed diverse behavior: AB linear diblock copolymers self-assembled into unilamellar vesicles, ABA linear triblock copolymers into cylindrical micelles, $(AB)_3$ 3-arm stars into spherical micelles, and cyclic graft copolymers into multilamellar vesicles [31]. Karatzas et al. [32] found that $(A)_2BC$ miktoarm star hybrid terpolypeptides preferentially formed polymersomes rather than core-shell micelles like their ABC linear analogues. Moreover, assemblies of star-shaped polymers also had a denser outer PEO corona, making them more resistant to enzymatic degradation [32].

Many effects of block copolymer architecture on the properties of self-assembled structures remain relatively unexplored. For example, because copolymers with different architectures are known to adopt distinct packing conformations within vesicle membranes [20,33,34], copolymer architecture is also expected to affect membrane thickness, stability, and permeability [35]. A recent meta-study [36] showed that ABA linear triblock copolymers containing a poly(dimethylsiloxane) (PDMS) block adopt more extended conformations within membranes than their AB diblock counterparts. Studying the same system, Itel et al. [37] also found that AB diblock copolymers formed thicker and more laterally mobile, weakly interdigitated bilayer membranes, while ABA triblock copolymers with a comparable number of PDMS units adopted a mix of bent U-shaped and stretched I-shaped conformations, reducing lateral mobility. However, analyses of this kind remain uncommon across different copolymer systems because relatively few self-assembly studies have systematically examined architectural effects, particularly beyond conventional AB and ABA linear block copolymers. Direct investigations into the relationship between copolymer architecture and self-assembly across a broader range of systems could therefore facilitate the rational design of polymersomes with improved control over membrane properties.

Here, poly(trimethylene carbonate-*b*-sarcosine) (P(TMC-*b*-Sar)) copolymers with AB linear diblock, ABA linear triblock, and AB_2 miktoarm star architectures were prepared by ring-opening polymerization (ROP), and their self-assembly in aqueous solution was studied. PTMC and PSar were selected as established biocompatible blocks [38,39], while PTMC additionally exhibits a glass transition temperature below room temperature ($T_g \approx -20$ °C) [40], providing enhanced flexibility to the hydrophobic block of the copolymer. The primary objective of this study was to evaluate how block copolymer architecture, together with structural parameters such as block length and block weight fraction, influences the morphology, size, population distribution, and membrane thickness of the resulting self-assembled nanostructures. The hydrophilic PSar weight fraction (f_{PSar}) was maintained at approximately 20–40 wt% to explore the compositional boundaries for polymersome formation. At the same time, the hydrophobic PTMC block length was restricted to 2.5–5.0 kDa to obtain vesicular membrane thicknesses comparable to those of biological cell membranes (8–10 nm) [7], while preserving polymersome stability.

2. Experimental

2.1. Characterization of block copolymers

2.1.1. Proton nuclear magnetic resonance (^{1}H NMR)

^{1}H NMR experiments were performed at room temperature using an AVANCE NEO 600 MHz NMR spectrometer (Bruker, USA) in dimethylsulfoxide-d_6 (≥99.8%; Eurisotop, France), with or without a few drops of trifluoroacetic acid (TFA; ≥99.5%; Thermo Fisher Scientific, USA). Tetramethylsilane (TMS; $\delta = 0$ ppm) was used as the internal chemical shift (δ) standard.

2.1.2. Size-exclusion chromatography coupled with multi-detection system consisting of multi-angle light scattering and differential refractive index detectors (SEC/MALS-RI)

SEC was performed in 0.05 M LiBr (≥99.0%; Sigma Aldrich, USA) in dimethylacetamide (DMAc; ≥99.9%; Riedel-de Haën, Germany) on a TSKgel ALPHA 3000 column (7.8 mm × 300 mm, 7 μm particle size; Tosoh Bioscience, Japan) with a precolumn at 50 °C. Samples were dissolved in the mobile phase at a concentration of 10 mg/mL. The

injected sample volume was 100 μL, and the flow rate was 0.4 mL/min. Detection was performed using a MALS detector (DAWN HELEOS II, Wyatt Technology, USA) and an RI detector (Optilab T-rEX, Wyatt Technology, USA). Toluene (≥99.7%; Riedel-de Haën, Germany) was used to calibrate the 90° LS detector, while the other detectors were normalized with standard polystyrene with a weight-average molar mass of 34 kDa and a dispersity of 1.04 (Polymer Standards Service, Germany). Calculation of the molecular weight characteristics of homo- and copolymers requires specific refractive index increments (*dn/dc*), which were determined from RI detector response, taking into consideration the known injected sample mass and assuming 100% mass recovery from the column. Data acquisition and evaluation were performed using ASTRA 8.2 software (Wyatt Technology, USA).

2.1.3. Gradient liquid adsorption chromatography (gLAC)

The presence of PSar and/or PTMC homopolymers in copolymer samples was investigated by gLAC using a ZORBAX Eclipse Plus C18 column (4.6 mm × 100 mm, 95 Å, 5 μm; Agilent Technologies, USA). Experiments were carried out on an Agilent Infinity 1260 HPLC system (USA) at room temperature. High-purity Milli-Q water with a resistivity of 18.2 MΩ·cm (MQ-water), supplemented with 0.1% (*v/v*) TFA (≥99.9%; Carl Roth, Germany), and tetrahydrofuran (THF; ≥99.9%; Riedel-de Haën, Germany) without stabilizer were used as solvents. The optimal solvent gradient was as follows: i) 0 to 0.5 min, 100% MQ-water; ii) 0.5 to 8 min, 100% to 0% MQ-water in THF; iii) 8 to 11 min, 100% THF; iv) 11 to 12 min, 0% to 100% MQ-water. Samples were dissolved at a concentration of 1 mg/mL in a mixture of acetonitrile (ACN; ≥99.9%; Riedel-de Haën, Germany) and MQ-water (ACN/MQ-water = 60:40, *v/v*) without TFA. The injection volume was 20 μL, and the flow rate was 1 mL/min. Detection was performed using an evaporative light scattering (ELS) detector (1260 Series, Agilent Technologies, USA). Agilent WinGPC 1.0 software was used for data acquisition and evaluation.

Residual PTMC homopolymer in copolymer samples was quantified with gLAC using a Nucleosil 100–5 OH (DIOL) column (4.6 mm × 250 mm, 100 Å, 5 μm; Macherey-Nagel, Germany). Experiments were performed on an Agilent Infinity 1260 HPLC system (USA) at 25 °C with ACN (≥99.9%; Riedel-de Haën, Germany) and MQ-water as solvents using the following gradient: i) 0 to 5 min, 100% ACN; ii) 5 to 30 min, 100% to 30% ACN in MQ-water; iii) 30 to 35 min, 30% ACN and 70% MQ-water; iv) 35 to 37 min, 30% to 100% ACN. Samples were dissolved in ACN at a concentration of 1 mg/mL. The injection volume was 100 μL, and the flow rate was 1 mL/min. Detection was performed using an RI detector (1260 Infinity, Agilent Technologies, USA). Chemstation B.04.03 with GPC Addon B.01.01 (Agilent Technologies, USA) software was used for data acquisition and evaluation.

2.2. Preparation of macromolecular dispersions

Macromolecular dispersions were prepared using thin-film rehydration procedure. Approximately 7.5 mg of copolymer was weighed into a 25 mL round-bottom flask and dissolved in 3 mL of $CHCl_3$ (≥99.8%; Merck, Germany). The solvent was slowly evaporated on a rotary evaporator to form a thin polymer film on the flask surface. The film was further dried in a desiccator overnight. To the dry film, 3 mL of 0.05 M $NaNO_3$ (≥99.5%; Merck, Germany) solution was added to form a dispersion, which was then stirred at 45 °C for 24 h. To homogenize the dispersion, it was first filtered through a 450 nm PTFE syringe filter (Merck, Germany) and then extruded through 200 nm and 100 nm polycarbonate membranes (Avanti Polar Lipids, USA) in two consecutive extrusions. Eleven membrane passes were performed during each extrusion.

To study the effect of PTMC homopolymer on P(TMC-*b*-Sar) copolymer self-assembly, two AB_2 copolymers and two AB copolymers were selected. Each copolymer was weighed into a round-bottom flask along with its corresponding PTMC homopolymer, which had been used in the copolymerization and would therefore closely resemble the main expected residual impurity. By dissolving both weighed polymers in $CHCl_3$, a thin film of copolymer with the target PTMC homopolymer content ($wt_{PTMC(HP)}$) was prepared (Table S1) and rehydrated to study the resulting self-assembly behavior.

2.3. Characterization of macromolecular dispersions

2.3.1. Batch dynamic light scattering (DLS)

Batch DLS measurements were performed in disposable microcuvettes (12.5 mm × 12.5 mm × 45 mm; Brand, Germany) on a Zetasizer Nano ZS instrument (Malvern Panalytical, UK) at 25 °C and a scattering angle of 173°. Data were processed with Zetasizer Software 8.02 (Malvern Panalytical, UK).

2.3.2. Asymmetric flow field-flow fractionation coupled with multi-detection system consisting of multi-angle light scattering, dynamic light scattering and differential refractive index detectors (AF4/MALS-DLS-RI)

AF4 separations were performed using an Eclipse NEON system with a Dilution Control Module (Wyatt Technology, USA), connected to an isocratic pump and autosampler (1260 Infinity II, Agilent Technologies, USA). The nanostructure populations in the samples were size-separated inside the Eclipse NEON Long Channel with a 350 μm fixed-height spacer, equipped with a regenerated cellulose membrane with a 10 kDa pore cutoff (Wyatt Technology, USA). A MALS detector with an embedded DLS module at a 141° scattering angle (DAWN HELEOS II, Wyatt Technology, USA) and an RI detector (Optilab T-rEX, Wyatt Technology, USA) were used for sample detection. The 90° MALS detector was calibrated with toluene (≥99.7%; Riedel-de Haën, Germany), while detectors at other angles were normalized with bovine serum albumin standard (2 mg/mL; Sigma Aldrich, USA). A solution of 0.05 M $NaNO_3$ (≥99.5%; Merck, Germany), supplemented with 0.02% (*w/v*) sodium azide (≥99.5%; Sigma Aldrich, USA), was used as the running eluent for all samples. Channel flow was set to 1 mL/min and detector flow to 0.3 mL/min. Two cross-flow gradients were used to separate nanostructures by size. After initially holding the cross-flow at 0.67 mL/min for 10 min, it was lowered linearly to 0.03 mL/min over 35 min in Gradient A, and exponentially to 0.03 mL/min over 45 min in Gradient B. Gradient B was used for samples containing nanostructures too large to fully elute during Gradient A. Data acquisition and evaluation were performed using ASTRA 8.2 software (Wyatt Technology, USA).

2.3.3. Cryogenic electron microscopy (cryo-EM)

Cryo-EM grids (Quantifoil® R 2/2, Quantifoil® R 2/1, or Lacey Carbon; Quantifoil, Germany) were first glow discharged in air using 20 mA current for 60 s (GloQube® Plus; Quorum Technologies, UK) to obtain a negatively charged hydrophilic surface. On a glow-discharged grid, 1.5 μL of macromolecular dispersion was deposited inside the Mark IV Vitrobot (Thermo Fisher Scientific, USA), where the grid was blotted twice under 100% humidity. A blot time of 8 s with a blot force value of 21 was used for the first blot, and a blot time of 4 s with a blot force value of 2 was used for the second blot. Immediately after blotting, the grid was plunged into liquid ethane. Electron micrographs were collected on a Glacios cryo-transmission electron microscope, operated at 200 kV and equipped with the Falcon 3 direct electron detector (Thermo Fisher Scientific, USA). Nominal magnifications of 5.3 kX, 45 kX, 57 kX, 73 kX, 92 kX, or 120 kX were used, with defocus set to −100 μm at 5.3 kX, and to −4 μm, −6 μm, or −8 μm at higher magnifications. Micrographs were collected using EPU 3.8 software (Thermo Fisher Scientific, USA), and membrane thickness measurements were performed using ImageJ 1.54 software and an in-house developed Python script (see Fig. S1 for explanation).

3. Results and discussion

3.1. Block copolymers

P(TMC-*b*-Sar) copolymers were synthesized by ROP of trimethylene carbonate (TMC) and sarcosine *N*-carboxyanhydride (Sar NCA), respectively (Figs. S2–S4). The structural parameters of both blocks were tuned by varying the initiator type (architecture) and the monomer-to-(macro)initiator ratio (block molecular weight) to study how these parameters influence copolymer self-assembly behavior. The amino end groups of PSar blocks were acetylated (Fig. 1) to prevent degradation of the ester bond between the PTMC block and glycine linker in AB and ABA copolymers during rehydration of the thin films at elevated temperature, and to ensure that all copolymer self-assembled nanostructures elute from the AF4 channel without adhering to the regenerated cellulose membrane.

SEC/MALS-RI chromatograms of P(TMC-*b*-Sar) copolymers show unimodal molecular weight distributions (Fig. S5) with low dispersity values ($Đ$ = 1.02–1.08; Table S2). The gLAC/ELS chromatograms of copolymers show the absence of PSar homopolymer; however, a certain amount of PTMC homopolymer is present in the P(TMC-*b*-Sar) (Fig. S6), probably due to initiation of ROP of TMC with water and/or inefficient initiation of ROP of Sar NCA from the macroinitiator amino groups. The content of PTMC homopolymer in the P(TMC-*b*-Sar) was evaluated by gLAC on a hydrophilic stationary phase column, with which the hydrophobic PTMC does not interact and elutes from the column immediately in the ACN isocratic region in SEC mode (Fig. S7). PTMC content in the copolymers was quantified with an RI detector using a calibration curve (Fig. S8). The number-average molecular weights of individual blocks and their fractions in the copolymers (Table 1) were determined from ^{1}H NMR spectra of the copolymers and the corresponding homopolymers (Figs. S9-S10), considering the content of PTMC in the copolymers as determined by HPLC with Eqs. (S6–S11).

Table 1
Characteristics of P(TMC-*b*-Sar) copolymers used to study their self-assembly behavior.

Architecture	Block copolymer label[a]	f_{PSar}[b] [%]	M_{PSar}[c] [kDa]	M_{PTMC}[d] [kDa]	$wt_{PTMC\ (HP)}$[e] [%]
AB	AB-17-4.6	17	0.9	4.6	9
	AB-19-2.6	19	0.6	2.6	10
	AB-21-2.5	21	0.7	2.5	2
	AB-21-4.4	21	1.2	4.4	8
	AB-27-4.4	27	1.6	4.4	7
	AB-28-2.5	28	1.0	2.5	2
	AB-33-2.6	33	1.3	2.6	2
	AB-33-4.0	33	2.0	4.0	4
	AB-39-2.5	39	1.6	2.5	2
ABA	ABA-19-3.7	19	0.9	3.7	< 1
	ABA-22-5.0	22	1.4	5.0	< 1
	ABA-32-5.0	32	2.3	5.0	< 1
AB_2	AB_2–18-2.8	18	0.6	2.8	6
	AB_2–24-2.5	24	0.8	2.5	11
	AB_2–24-3.5	24	1.1	3.5	13
	AB_2–24-5.0	24	1.6	5.0	30
	AB_2–28-2.6	28	1.0	2.6	5
	AB_2–35-3.5	35	1.9	3.5	8
	AB_2–36-2.7	36	1.5	2.7	11
	AB_2–38-2.5	38	1.5	2.5	18
	AB_2–38-4.5	38	2.7	4.5	17

[a] The labels indicate information on architecture, f_{PSar} [%], and M_{PTMC} [kDa].
[b] The PSar block weight fraction, determined by ^{1}H NMR and calculated with Eq. (S8), accounting for the PTMC homopolymer content.
[c] The molecular weight of the PSar block, determined by ^{1}H NMR and calculated with Eq. (S10), accounting for the PTMC homopolymer content.
[d] The molecular weight of the PTMC block, determined by ^{1}H NMR of the corresponding PTMC homopolymer used for copolymer synthesis and calculated with Eq. (S11).
[e] Residual PTMC homopolymer content, given as the weight fraction in P(TMC-*b*-Sar), determined by gLAC/RI on a hydrophilic stationary phase column using the calibration curve (Fig. S8).

3.2. Morphology and size distribution of self-assembled structures of architecturally different P(TMC-b-Sar) copolymers

Dispersions of P(TMC-*b*-Sar) copolymers were prepared by thin-film rehydration, then filtered and extruded in three consecutive steps. Size homogenization was performed to remove populations with larger diameters, such as giant unilamellar and large multivesicular vesicles. The formed supramolecular structures were characterized with batch DLS to rapidly screen the average structure size and dispersity, AF4/MALS-DLS-RI to provide information about size distribution and the relative concentration of populations of different sizes, and cryo-EM to thoroughly evaluate aggregate morphology, including various anomalous features and finer details, such as vesicle membrane thickness.

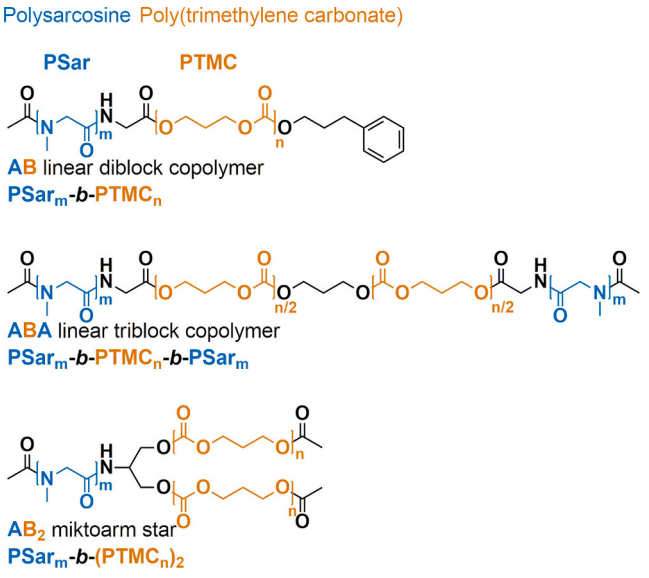

Fig. 1. P(TMC-*b*-Sar) chemical structures for AB linear diblock, ABA linear triblock, and AB_2 miktoarm star architectures.

When comparing P(TMC-*b*-Sar) copolymers of AB linear and AB_2 miktoarm star architectures with PTMC block molecular weights (M_{PTMC}) of approximately 2.5 kDa, AB_2 miktoarm stars formed polymersomes over a wider range of PSar block weight fractions. At the lowest tested f_{PSar} of 19%, the AB copolymer AB-19-2.6 formed predominantly vesicles with fewer spherical micelles (Fig. 2a), whereas the miktoarm star AB_2–18-2.8 with a comparable 18% f_{PSar} formed exclusively vesicles without spherical micelles (Fig. 2f). As the hydrophilic block length increased, the dispersion of AB-21-2.5 with 21% f_{PSar} already contained a significant fraction of spherical micelles alongside polymersomes (Fig. 2b), whereas AB_2–24-2.5 with a slightly higher 24% f_{PSar} still formed polymersomes as the dominant morphology (Fig. 2g). The copolymer AB-28-2.5 with 28% f_{PSar} self-assembled mostly into micelles, including many cylindrical ones (Fig. 2c). In contrast, AB_2–28-2.6 formed a heterogeneous mixture of vesicles, spherical micelles, and fewer cylindrical micelles (Fig. 2h), which were also thinner than those formed by the aforementioned AB linear analogue (Fig. 2c). Consistent with vesicle formation over a broader range of f_{PSar}, AB_2 copolymers formed the highest number of cylindrical micelles at higher f_{PSar} values close to 35% (Fig. 2i), although AB_2–38-2.5 with a slightly higher 38% f_{PSar} (Fig. 2j) formed predominantly spherical micelles. The number of cylindrical micelles formed from AB copolymers began to decrease above 30% f_{PSar} (Fig. 2d), and exclusively spherical micelles were observed in the dispersion of AB-39-2.5 with 39% f_{PSar} (Fig. 2e).

Differences in self-assembly behavior between AB and AB_2

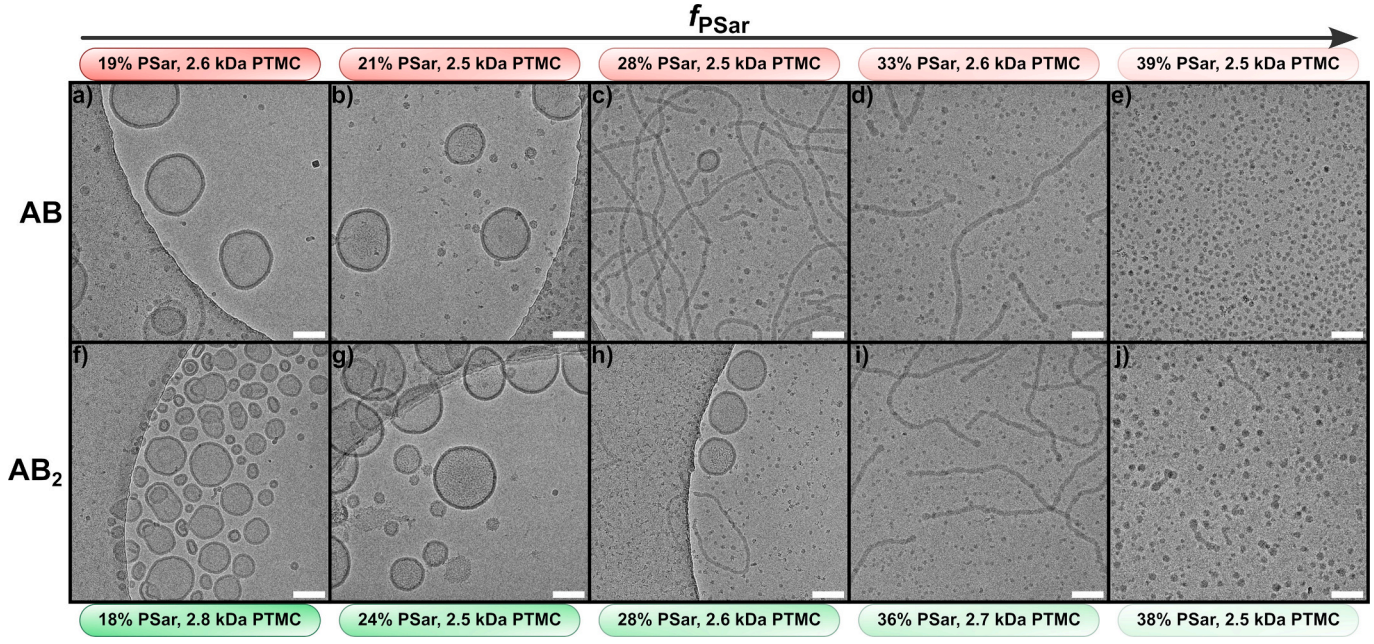

Fig. 2. Cryo-EM micrographs at 73 kX magnification show dispersions prepared from P(TMC-*b*-Sar) copolymers with AB and AB_2 architectures, where the molecular weight of the PTMC block is similar (close to 2.5 kDa). Micrographs are arranged from left to right in order of increasing PSar block weight fractions, separately for each architecture. White scale bars represent 100 nm.

copolymers can be explained by the packing parameter ($p = v/a_0 l_c$). Assuming nearly equal molecular weights of hydrophilic and hydrophobic blocks in AB and AB_2 copolymers, their values for v and a_0 are very similar, while l_c for the AB_2 copolymer is half that of the AB copolymer. Therefore, the p value of the AB_2 copolymer is higher, indicating vesicle formation over a wider range of hydrophilic block weight fractions [18,25]. Additionally, it has been proposed that the AB_2 architecture can lead to greater lateral crowding between neighboring hydrophobic chains, causing them to stretch more than in linear copolymers [18,25,29]. This energetically unfavorable behavior is reduced in self-assembled structures with lower interfacial curvature, which is why AB_2 copolymers tend to form vesicles even at higher hydrophilic block weight fractions [18,25,29].

The size distribution of nanostructure populations was assessed using the AF4/MALS-DLS-RI technique. For example, the fractogram of the AB-21-2.5 copolymer dispersion shows a main RI peak in the elution time range of 36–60 min and an additional narrower RI peak with apex at elution time of ~23 min (Fig. 3). Together with cryo-EM (Fig. 2b), MALS detector response, and measured R_h values as a function of elution time, the earlier eluting species of AB-21-2.5 can be attributed to spherical micelles, while the main peak corresponds to vesicles. Conversely, the fractogram of AB_2–24-2.5 shows a single RI peak with an apex at ~47 min and significant fronting in the elution time range of 20–40 min (Fig. 3). The earlier eluting species of AB_2–24-2.5 indicate the presence of smaller vesicles in the 30–100 nm diameter range, which is consistent with cryo-EM observations (Fig. 2g) and was also observed for other miktoarm stars, such as AB_2–18-2.8 (Fig. 2f) and AB_2–24-3.5 (Fig. 4e). The formation of smaller vesicles with higher membrane curvature from AB_2 copolymers could be attributed to the higher elasticity of the membrane, specifically the bending modulus, which was previously proposed to depend on copolymer architecture [41].

Increasing the length of the PTMC block affects the self-assembly behavior of P(TMC-*b*-Sar) block copolymers with AB architecture. The formation of structures with higher interfacial curvature (e.g., micelles) was more favored in copolymers with ~4.0 kDa M_{PTMC} than in those with ~2.5 kDa M_{PTMC}. For example, copolymer AB-33-4.0 formed spherical micelles without worm-like morphologies (Fig. 4d), which were present in the dispersion of its shorter PTMC block analogue AB-33-2.6 (Fig. 2d). Similarly, copolymer AB-27-4.4 formed cylindrical and spherical micelles, with no vesicles observed (Fig. 4b). Following the same trend, unilamellar vesicles very rarely formed from copolymer AB-21-4.4 with 4.4 kDa M_{PTMC} (Fig. 4c) compared to the shorter PTMC block analogue AB-21-2.5 with 2.5 kDa M_{PTMC} (Fig. 2b). Instead, AB-21-4.4 formed a complex mixture of spherical and cylindrical micelles, branched cylindrical micelles, interconnected micellar networks, and structures resembling perforated vesicles (stomatosomes; Fig. 4c). These unusual branched micellar structures are thought to form through entanglement of longer cylindrical micelles of specific amphiphiles [42], and have also been observed for block copolymers in previous studies

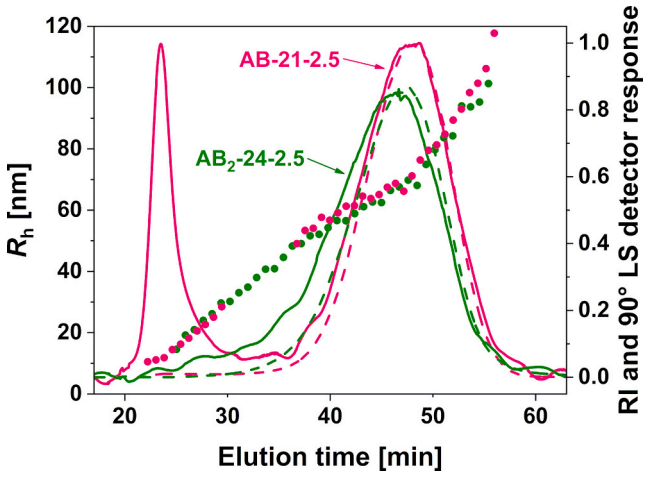

Fig. 3. AF4 fractograms of dispersions prepared from copolymers with AB (AB-21-2.5; magenta curves and symbols) and AB_2 (AB_2–24-2.5; green curves and symbols) architectures. Both dispersions were extruded through a polycarbonate membrane with a 100 nm pore size. Solid curves represent the refractive index detector response, dashed curves represent the 90° light scattering detector response, and round symbols show the hydrodynamic radius as a function of elution volume. (For interpretation of the references to colour in this figure legend, the reader is referred to the web version of this article.)

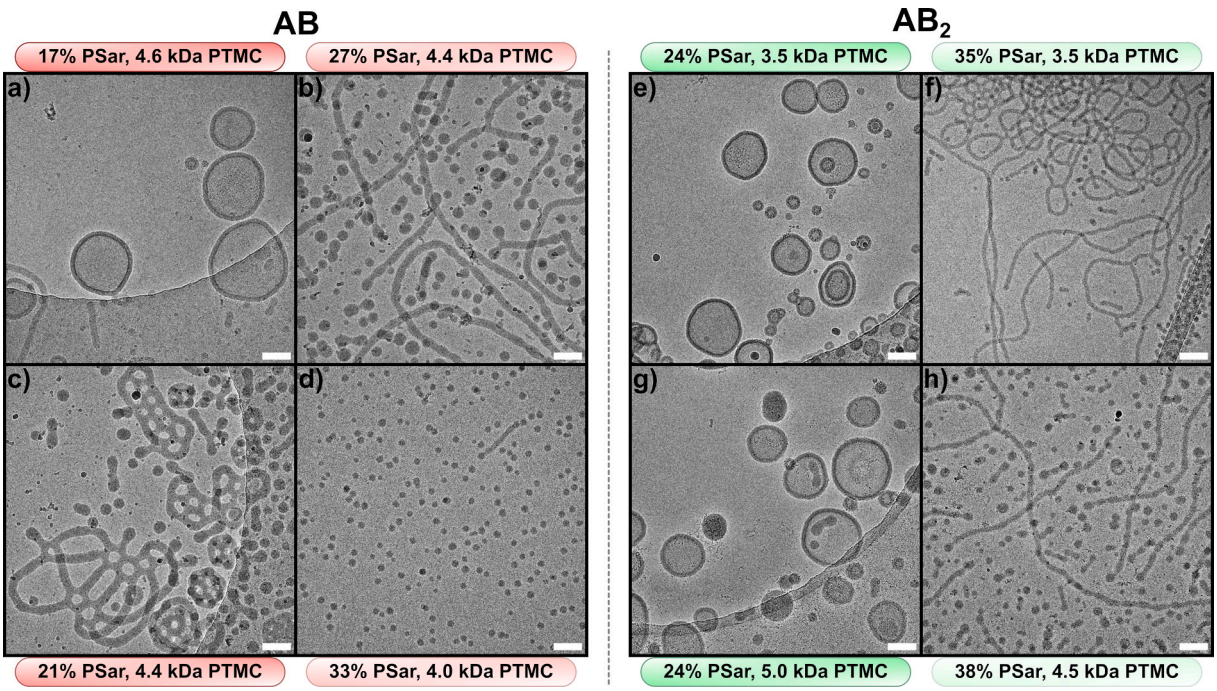

Fig. 4. Cryo-EM micrographs at 57 kX magnification show dispersions prepared from P(TMC-*b*-Sar) copolymers with AB and AB_2 architectures, where the molecular weight of the PTMC block is equal to or greater than 3.5 kDa. Micrographs are grouped by copolymer architecture and displayed with lower PSar block weight fractions on the left. White scale bars represent 100 nm.

[22,43–45].

The self-assembly of linear AB diblock P(TMC-*b*-Sar) copolymers appears largely consistent with that of PEO-*b*-PTMC analogues, for which Lebleu et al. [46] found optimal polymersome formation at approximately 17% f_{PEO} and 9 kDa M_{PTMC}. Although the block molecular weights of P(TMC-*b*-Sar) with the AB architecture studied here were at least two times lower, an f_{PSar} of 21% was likely still too high for optimal polymersome formation, especially when M_{PTMC} was above 4.0 kDa (Fig. 4c). Lowering f_{PSar} below 20% enabled reliable polymersome formation from AB-17-4.6, even with a longer 4.6 kDa PTMC block (Fig. 4a). Other examples of copolymer block lengths affecting self-assembly have been reported. Qi et al. [47] observed a similar trend in the self-assembly of linear AB diblock poly(ethylene oxide)-*b*-poly (ε-caprolactone) (PEO-*b*-PCL) copolymers prepared by thin-film rehydration. Keeping f_{PEO} constant at 15%, they identified vesicles as the dominant morphology up to 15 kDa M_{PCL}, but observed them only rarely at M_{PCL} above 20 kDa. Jain and Bates [43] studied poly(ethylene oxide)-*b*-poly(butadiene) (PEO-*b*-PBD) copolymers that also behaved similarly. Various cylindrical micellar structures, including loops, Y-junctions, and networks, formed more readily alongside or instead of vesicles when the copolymer blocks were longer at the same hydrophilic block fraction [43].

In contrast to the P(TMC-*b*-Sar) copolymers with AB architecture, counterparts with AB_2 architecture and a fixed 24% f_{PSar} did not show a similar effect of M_{PTMC} on the morphology of self-assembled structures. Like their shorter PTMC block analogue AB_2–24-2.5 with 2.5 kDa M_{PTMC} (Fig. 2g), copolymers AB_2–24-3.5 with 3.5 kDa M_{PTMC} (Fig. 4e) and AB_2–24-5.0 with 5.0 kDa M_{PTMC} (Fig. 4g) also primarily formed polymersomes. When f_{PSar} was increased to 35%, cylindrical and spherical micelles formed from AB_2–35-3.5 with 3.5 kDa M_{PTMC} (Fig. 4f), which is comparable to AB_2–36-2.7 with 2.7 kDa M_{PTMC} (Fig. 2i). Notably, copolymer AB_2–38-4.5 with 38% f_{PSar} and 4.5 kDa M_{PTMC} also formed both cylindrical and spherical micelles (Fig. 4h), which differed from AB_2–38-2.5 with the same f_{PSar} and 2.5 kDa M_{PTMC}, which formed predominantly spherical micelles (Fig. 2j).

Among ABA linear triblock P(TMC-*b*-Sar) copolymers, ABA-19-3.7 with 19% f_{PSar} and ABA-22-5.0 with 22% f_{PSar} both formed polymersomes as the dominant morphology (Figs. S11a–S11b). ABA-32-5.0 with 32% f_{PSar} self-assembled into spherical and cylindrical micelles (Fig. S11c). Overall, micelles were less frequent in dispersions formed from ABA copolymers with approximately 20% f_{PSar} (Figs. S11a–S11b) than in dispersions of comparable AB copolymers (Figs. 2a, b, and 4c). This suggests superior vesicle formation by the linear triblock architecture compared to the linear diblock. In addition, polymersomes from ABA copolymers were morphologically more similar to those formed from AB copolymers, with fewer multivesicular species and smaller vesicles than in dispersions formed from AB_2 copolymers.

3.3. *Influence of PTMC homopolymers on the self-assembly of P(TMC-b-Sar) copolymers*

P(TMC-*b*-Sar) copolymers contained different amounts of residual PTMC homopolymer from synthesis, raising the question of how PTMC homopolymer affects the self-assembly behavior of the copolymers. The fractogram of copolymer AB_2–18-2.8 without added PTMC homopolymer before thin-film rehydration shows a wide elution time range of 25–55 min (Fig. 5a), including a predominant population in the smaller 30–100 nm diameter range. These results correspond with the cryo-EM, where a clear distribution in vesicle size was observed (Fig. 5b). With the addition of PTMC homopolymer up to 18% total $wt_{PTMC(HP)}$, the RI detector response in the elution time range of 20–40 min became negligible, and the main peak shifted toward longer retention time (Fig. 5a). This indicates the formation of larger structures with densely partitioned vesicular morphology, as observed by cryo-EM (Fig. 5b), which suggests that smaller vesicles become prone to aggregation as the homopolymer content in the initial copolymer thin film increases. This hypothesis is supported by the presence of possible intermediate structures, such as clustered vesicles, in the dispersion with 12% $wt_{PTMC(HP)}$ (Fig. 5b). Similar observations were made for AB_2–24-3.5, which contained a higher initial PTMC homopolymer content of 13% (Figs. 5c–5d). While this copolymer appeared less prone to forming densely partitioned vesicular structures, these structures became abundant, though not

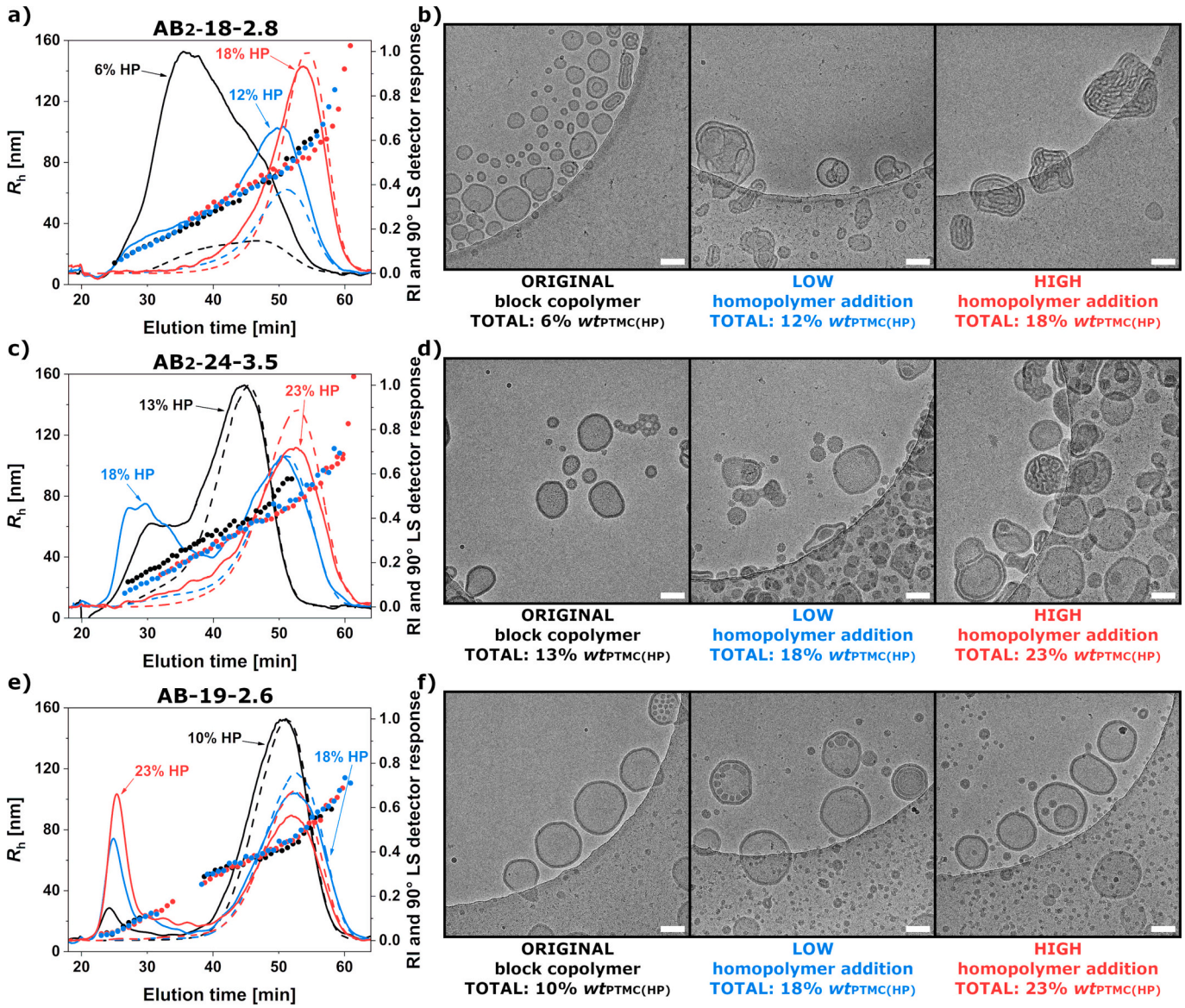

Fig. 5. a), c), and e): AF4 fractograms of macromolecular dispersions prepared from copolymers **a)** AB_2–18-2.8, **c)** AB_2–24-3.5, and **e)** AB-19-2.6, without the addition of the corresponding PTMC homopolymer (black curves and symbols), and with a low (blue curves and symbols) or high (red curves and symbols) amount of PTMC homopolymer added during thin-film preparation. All analyzed dispersions were extruded through a polycarbonate membrane with a 100 nm pore size. Solid curves represent the refractive index detector response, dashed curves represent the 90° light scattering detector response, and round symbols show the hydrodynamic radius as a function of elution time. **b), d), and f):** Cryo-EM micrographs at 57 kX magnification of supramolecular structures formed from copolymers **b)** AB_2–18-2.8, **d)** AB_2–24-3.5, and **f)** AB-19-2.6 without the addition of the corresponding PTMC homopolymer (left micrograph), and with a low (middle micrograph) or high (right micrograph) amount of PTMC homopolymer added during thin-film preparation. All imaged dispersions were extruded through a polycarbonate membrane with a 100 nm pore size. White scale bars represent 100 nm.

dominant, at 23% $wt_{PTMC(HP)}$ (Fig. 5d). Many other types of clustered structures were also present in both dispersions with 18% and 23% $wt_{PTMC(HP)}$. Overall, vesicles with smaller diameters seem much more susceptible to homopolymer-induced aggregation, which could explain why copolymer AB_2–18-2.8 exhibited this behavior more strongly, as it naturally forms vesicles in a smaller size range than AB_2–24-3.5.

The vesicular morphology was significantly less affected after adding PTMC homopolymer to copolymers AB-19-2.6 and AB-21-2.5, which both behaved similarly at the highest tested homopolymer content of 23% $wt_{PTMC(HP)}$ (Figs. 5e, 5f, and S12). Most vesicles remained unilamellar, and only a small number of aggregated structures were observed (Figs. 5f and S12). Vesicle formation decreased at higher levels of PTMC homopolymer, as AF4 fractograms showed a reduction in the RI detector response at longer elution times (~50 min; Fig. 5e). Additionally, more structures in the size range of copolymer micelles and smaller vesicles formed, as the RI detector response at ~25 min increased with higher $wt_{PTMC(HP)}$. These smaller spherical structures could possibly contain the poorly soluble PTMC homopolymer, stabilized by an outer copolymer layer with hydrophilic PSar chains exposed at the surface. Incorporation of the hydrophobic homopolymer into copolymer micelles was previously proposed in an earlier study on polystyrene-*b*-polyacrylic acid (PS-*b*-PAA) by Zhang and Eisenberg [48], and in a theoretical study by Linse [49], where PPO homopolymer impurity at 5% volume fraction could make up to 10% of the PEO-*b*-PPO-*b*-PEO micellar volume. A proportion of PTMC homopolymer also appears to be incorporated into the hydrophobic membrane interior of the vesicles from both AB and AB_2 copolymers, as indicated by the increase in membrane thickness with increasing $wt_{PTMC(HP)}$ (Table S3).

Overall, these results suggest that the self-assembly of the AB copolymers used in this study was not significantly affected by the residual

PTMC homopolymer content, which ranged from 2 to 10% (Table 1). Some synthesized AB_2 copolymers contained larger amounts of PTMC homopolymer that could influence self-assembly behavior; however, these effects seem to become significant only at levels of ~20% $wt_{PTMC(HP)}$. Among the copolymers studied, AB_2–38-2.5 and AB_2–38-4.5 are close to this value (Table 1), but due to their high 38% f_{PSar} content, they only formed micelles (Figs. 2j and 4h), which were much less affected morphologically by the PTMC homopolymer than vesicles. Copolymer AB_2–24-5.0 was an outlier, as it still primarily formed unilamellar vesicles despite a very high 30% $wt_{PTMC(HP)}$ (Fig. 4g), possibly due to higher M_{PTMC} compared to other AB_2 copolymers. Nevertheless, the high concentration of PTMC homopolymer in this dispersion is evident from the presence of some vesicles with unevenly thickened membranes and large non-hollow spherical homopolymer aggregates that could reach ~100 nm in diameter (Fig. 4g). Several other AB_2 copolymers with $wt_{PTMC(HP)}$ above 20% showed more severe morphological changes to the vesicles and were therefore not included in the final self-assembly study (Fig. S13).

3.4. Membrane thickness of polymersomes

Membranes of polymersomes formed from block copolymers with various architectures were evaluated by measuring their thickness. The membrane thickness (d) increased primarily with the length of the hydrophobic PTMC block (Table 2), consistent with other block copolymer systems [2,50]. Regarding architectural differences, copolymer ABA-19-3.7 formed a thinner membrane at 3.7 kDa M_{PTMC} (~9.4 nm; Table 2) than copolymers AB-21-2.5 and AB_2–24-2.5 at approximately 2.5 kDa M_{PTMC} (~11.3 nm and ~ 10.2 nm, respectively; Table 2). This likely indicates that ABA copolymers primarily span the membrane in an I-shape, forming a monolayer. In contrast, AB and AB_2 copolymers presumably form comparatively thicker interdigitated membrane structures [34]. The thickness of membranes from AB and AB_2 copolymers at ~2.5 kDa M_{PTMC} is therefore more appropriate for comparison to ABA membranes from ABA-22-5.0 with twice their M_{PTMC} value of 5.0 kDa. Moreover, controlled synthesis of ABA copolymers with low molecular weight can be difficult due to the low number of PSar units on each side of the central PTMC block.

The thickness of membranes from AB_2 miktoarm stars with ~2.5 kDa M_{PTMC} was approximately 10–20% lower than that of membranes from AB copolymers (Table 2). The thinner vesicle membrane formed from the AB_2 copolymer aligns with expectations, as the hydrophobic block of the AB_2 copolymer is theoretically half the length of its AB analogue at the same M_{PTMC}. However, the actual measured difference in membrane thickness between the two architectures was much less than a factor of two, since the PTMC chains did not adopt a fully extended conformation within the membrane. For full extension to occur, the hydrophobic chains of different block copolymer molecules would need to demix, which is entropically unfavorable and has not been observed for block copolymers in general, either experimentally or in simulations [33,34,51]. In fact, based on the previously studied PEO_{45}-*b*-$PTMC_{96}$ copolymer [46], Effenberg and Gaitzsch [36] recently calculated that the degree of chain stretching was only 4%, indicating that the PTMC chains within that membrane would be almost entirely in the random coil conformation. Shorter hydrophobic chains, like those studied here, tend to coil less due to the greater proximity of hydrophilic groups within the membrane [36,37,52]. This effect could reduce the difference in membrane thickness between the AB and AB_2 architecture copolymers, as the latter contain two shorter, but possibly more stretched, PTMC chains.

Table 2
Membrane thickness of polymersomes prepared from copolymers with different macromolecular architectures, PTMC block molecular weights (M_{PTMC}), and residual PTMC homopolymer weight fractions ($wt_{PTMC(HP)}$).

Block copolymer label	M_{PTMC} [kDa]	$wt_{PTMC(HP)}$ [%]	d[a] [nm]
AB-21-2.5	2.5	2	11.3 ± 1.0
AB-28-2.5	2.5	2	11.0 ± 1.2
AB-19-2.6	2.6	10	12.1 ± 1.1
AB-17-4.6	4.6	9	15.9 ± 1.1
ABA-19-3.7	3.7	< 1	9.4 ± 0.8
ABA-22-5.0	5.0	< 1	12.6 ± 1.1
AB_2–24-2.5	2.5	11	10.2 ± 1.0
AB_2–28-2.6	2.6	5	10.4 ± 1.0
AB_2–18-2.8	2.8	6	9.4 ± 0.8
AB_2–24-3.5	3.5	13	12.5 ± 1.2
AB_2–24-5.0	5.0	30	15.3 ± 1.7

[a] Membrane thickness, presented as the mean value ± standard deviation of all measurements from cryo-EM micrographs.

Data from the homopolymer study suggest that the effect of PTMC homopolymer on membrane thickness is more pronounced for AB copolymers (Table S3). However, when comparing the polymersome membrane thickness of copolymers AB-21-2.5 and AB-19-2.6 (~11.3 nm at 2% $wt_{PTMC(HP)}$ and ~12.1 nm at 10% $wt_{PTMC(HP)}$, respectively; Table 2), the effect of the homopolymer is detectable but falls within the standard deviation of both measurements. With the possible exception of AB_2–24-5.0 with 30% $wt_{PTMC(HP)}$, the effect of PTMC homopolymer on membrane thickness was likely marginal for AB_2-derived polymersomes and outweighed by other variables. For example, AB_2–18-2.8 formed a thinner membrane (~9.4 nm; Table 2) than AB_2–28-2.6 (~10.4 nm; Table 2) despite having a slightly longer PTMC block and similar $wt_{PTMC(HP)}$, which could be related to AB_2–18-2.8 forming vesicles in a smaller size range or to differences in the molecular weight of the hydrophilic block [2].

3.5. Temperature stability of polymersomes

The stability of polymersomes is an important factor for their application. In this study, stability was evaluated over 2 months under different storage conditions: i) in a refrigerator at 5 °C, ii) at room temperature, and iii) in an incubator at 40 °C. Dispersions were sampled and characterized at predetermined time intervals. Regardless of copolymer architecture, the results show minimal changes in measured R_h and radius of gyration (R_g; Table S4) of polymersomes after 2 months at 5 °C or room temperature, indicating that they remain stable for at least 2 months under typical storage conditions. Morphological and size distribution changes were also minimal (Figs. 6a and 6c).

Conversely, changes in polymersomes were observed when they were stored at 40 °C. For polymersomes from the AB copolymer AB-21-2.5, the measured R_h and R_g decreased by about 15 nm after 1 month (Table S4). This change is also evident in the AF4 fractogram, where the main peak shifted to shorter elution times, while the RI signal peak for the micelle population became less intense relative to the main peak and shifted toward longer elution times (Fig. 6a), indicating a smaller fraction of somewhat larger micelle populations. The membrane thickness increased markedly from approximately 11 nm to 16 nm (Fig. 6b). After 2 months, R_h and R_g decreased by another 8 nm (Table S4), and the micelle peak disappeared entirely from the AF4 fractogram (Fig. 6a). Cryo-EM revealed spherical structures with thick (> 20 nm) and uneven walls surrounding reduced lumens (Fig. 6b). Simple tomographic observations at two angles confirmed that these structures were indeed spherical in 3D space and not indented or deformed in some other way (Fig. S14).

In comparison, polymersomes from the AB_2 copolymer AB_2–24-2.5 at 40 °C showed less morphological change after 1 month, with membrane thickness increasing by around 1.5 nm (Fig. 6d), although measured R_h and R_g still decreased by 8 nm and 10 nm, respectively (Table S4). Both radii were further reduced after 2 months (Fig. 6c and Table S4), and the morphological changes became much more pronounced. Spheroidal structures with wall thickness varying greatly from 11 nm to 40 nm were observed (Fig. 6d), ultimately suggesting a similar morphological transition to the AB copolymer under these conditions,

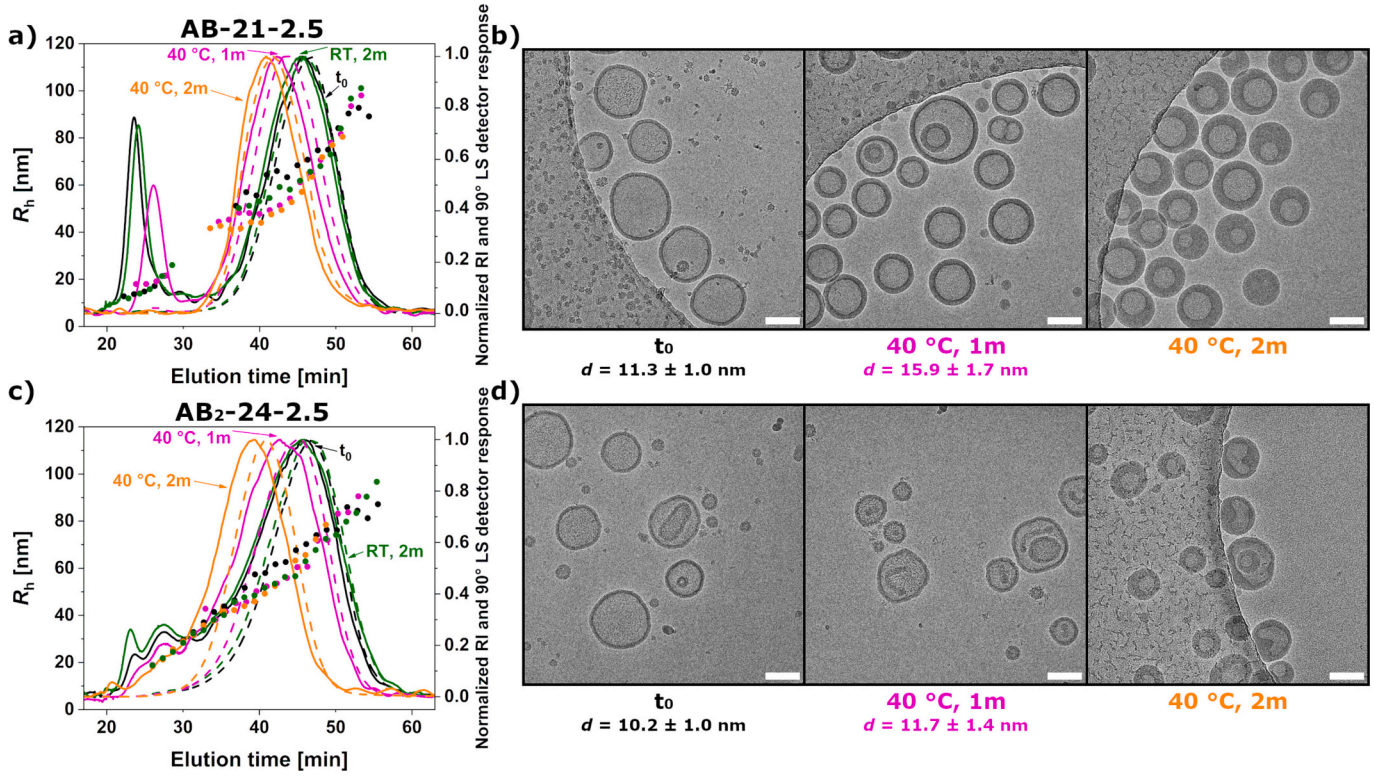

Fig. 6. a) and c): AF4 fractograms of macromolecular dispersions prepared from **a)** AB copolymer AB-21-2.5 and **c)** AB_2 copolymer AB_2–24-2.5 at starting time t_0 (black curves and symbols), and after aging for 2 months at room temperature (RT; green curves and symbols), 1 month at 40 °C (magenta curves and symbols), or 2 months at 40 °C (orange curves and symbols). All analyzed dispersions were extruded through a polycarbonate membrane with a 100 nm pore size. Solid curves represent the normalized refractive index detector response, dashed curves represent the normalized 90° light scattering detector response, and round symbols show the hydrodynamic radius as a function of elution time. **b) and d):** Cryo-EM micrographs at 73 kX magnification of supramolecular structures formed from **b)** AB copolymer AB-21-2.5 and **d)** AB_2 copolymer AB_2–24-2.5 at starting time t_0 (left micrograph), and aged at 40 °C for 1 month (middle micrograph) or 2 months (right micrograph). All imaged dispersions were extruded through a polycarbonate membrane with a 100 nm pore size. White scale bars represent 100 nm.

but at a slower rate. While these morphological changes would require further investigation to fully understand mechanistically, it is clear that they progress slowly over weeks and months, meaning that most practical applications of P(TMC-*b*-Sar) polymersomes at slightly elevated temperatures would still be feasible.

4. Conclusions

In summary, the macromolecular architecture of newly prepared P(TMC-*b*-Sar) copolymers influences the formation of supramolecular structures in aqueous solution, which remain stable for at least two months at room temperature. AB_2 miktoarm stars consistently form polymersomes up to ~28% f_{PSar} as investigated in this study, whereas their AB linear counterparts do so within a more limited range near 20% f_{PSar}, which narrows further with increasing M_{PTMC}. In addition, AB_2 copolymers preferentially form a greater population of smaller vesicles (30–100 nm diameter) and produce membranes that are approximately 10–20% thinner than those formed by AB copolymers. At comparable M_{PTMC} values, these observations suggest that the two shorter PTMC chains in the miktoarm star architecture adopt a more extended conformation within membrane relative to the single longer PTMC chain of the AB analogues, while the low membrane thickness of ABA copolymers is indicative of monolayer formation.

The synthesis procedures used to prepare P(TMC-*b*-Sar) copolymers with different architectures resulted in varying amounts of residual PTMC homopolymer. Quantification of this hydrophobic impurity proved essential for accurately determining copolymer composition and understanding its influence on self-assembly behavior. Morphologically, smaller vesicles formed by miktoarm star copolymers were particularly sensitive to PTMC homopolymer content, exhibiting aggregation when the PTMC homopolymer fraction approached ~20 wt%.

Overall, this study demonstrates the potential of alternative copolymer architectures, particularly AB_2 miktoarm stars, to direct the formation of self-assembled structures with tailored morphology, size distribution, and membrane properties. The results also highlight the sensitivity of block copolymer self-assembly to synthesis-related impurities, which are rarely quantified but warrant greater consideration in the development of emerging block copolymer systems. These findings provide a foundation for future investigations into the relationships between copolymer architecture, membrane structure, and functional properties, including the incorporation of membrane proteins into polymersomes formed from architecturally distinct copolymers.

CRediT authorship contribution statement

Aljaž Pogorelec: Writing – original draft, Visualization, Methodology, Investigation, Formal analysis, Data curation. **Urška Češarek:** Writing – review & editing, Visualization, Methodology, Investigation. **Blaž Zdovc:** Writing – review & editing, Visualization, Investigation. **Ema Žagar:** Writing – review & editing, Supervision, Methodology, Funding acquisition, Conceptualization. **David Pahovnik:** Writing – review & editing, Supervision, Methodology, Funding acquisition, Conceptualization.

Declaration of competing interest

The authors declare that they have no known competing financial interests or personal relationships that could have appeared to influence

the work reported in this paper.

Acknowledgements

The authors acknowledge the financial support from the Slovenian Research and Innovation Agency, namely research core funding P2-0145 and project J2-4438. Cryo-EM observations were performed at the National Institute of Chemistry Cryo-EM facility. The authors would also like to thank Matic Kisovec for technical assistance with the electron microscope.

Appendix A. Supplementary data

Supplementary data to this article can be found online at https://doi.org/10.1016/j.jcis.2026.141238.

Data availability

Data will be made available on request.

References

[1] D. Lombardo, M.A. Kiselev, S. Magazù, P. Calandra, Amphiphiles self-assembly: basic concepts and future perspectives of supramolecular approaches, Adv. Condens. Matter Phys. 2015 (2015) 1–22, https://doi.org/10.1155/2015/151683.
[2] Y. Mai, A. Eisenberg, Self-assembly of block copolymers, Chem. Soc. Rev. 41 (2012) 5969–5985, https://doi.org/10.1039/c2cs35115c.
[3] H. Feng, X. Lu, W. Wang, N.-G. Kang, J.W. Mays, Block copolymers: synthesis, self-assembly, and applications, Polymers 9 (2017) 494, https://doi.org/10.3390/polym9100494.
[4] A. Blanazs, S.P. Armes, A.J. Ryan, Self-assembled block copolymer aggregates: from micelles to vesicles and their biological applications, Macromol. Rapid Commun. 30 (2009) 267–277, https://doi.org/10.1002/marc.200800713.
[5] M. Karayianni, S. Pispas, Block copolymer solution self-assembly: recent advances, emerging trends, and applications, J. Polym. Sci. 59 (2021) 1874–1898, https://doi.org/10.1002/pol.20210430.
[6] K.E.B. Doncom, L.D. Blackman, D.B. Wright, M.I. Gibson, R.K. O'Reilly, Dispersity effects in polymer self-assemblies: a matter of hierarchical control, Chem. Soc. Rev. 46 (2017) 4119–4134, https://doi.org/10.1039/C6CS00818F.
[7] E. Rideau, R. Dimova, P. Schwille, F.R. Wurm, K. Landfester, Liposomes and polymersomes: a comparative review towards cell mimicking, Chem. Soc. Rev. 47 (2018) 8572–8610, https://doi.org/10.1039/C8CS00162F.
[8] D.E. Discher, A. Eisenberg, Polymer vesicles, Science 297 (2002) 967–973, https://doi.org/10.1126/science.1074972.
[9] F. Meng, Z. Zhong, J. Feijen, Stimuli-Responsive Polymersomes for Programmed Drug Delivery, Biomacromolecules 10 (2009) 197–209, https://doi.org/10.1021/bm801127d.
[10] X. Hu, Y. Zhang, Z. Xie, X. Jing, A. Bellotti, Z. Gu, Stimuli-responsive Polymersomes for biomedical applications, Biomacromolecules 18 (2017) 649–673, https://doi.org/10.1021/acs.biomac.6b01704.
[11] C.G. Palivan, R. Goers, A. Najer, X. Zhang, A. Car, W. Meier, Bioinspired polymer vesicles and membranes for biological and medical applications, Chem. Soc. Rev. 45 (2016) 377–411, https://doi.org/10.1039/C5CS00569H.
[12] P. Chen, M. Qiu, C. Deng, F. Meng, J. Zhang, R. Cheng, Z. Zhong, pH-responsive Chimaeric Pepsomes based on asymmetric poly(ethylene glycol)-b-poly(l-leucine)-b-poly(l-glutamic acid) triblock copolymer for efficient loading and active intracellular delivery of doxorubicin hydrochloride, Biomacromolecules 16 (2015) 1322–1330, https://doi.org/10.1021/acs.biomac.5b00113.
[13] S. Moreno, S. Boye, H.G.A. Ajeilat, S. Michen, S. Tietze, B. Voit, A. Lederer, A. Temme, D. Appelhans, Multivalent protein-loaded pH-stable Polymersomes: first step toward protein targeted therapeutics, Macromol. Biosci. 21 (2021) 2100102, https://doi.org/10.1002/mabi.202100102.
[14] M. Kumar, M. Grzelakowski, J. Zilles, M. Clark, W. Meier, Highly permeable polymeric membranes based on the incorporation of the functional water channel protein aquaporin Z, PNAS 104 (2007) 20719–20724, https://doi.org/10.1073/pnas.0708762104.
[15] L. Klermund, S.T. Poschenrieder, K. Castiglione, Biocatalysis in Polymersomes: improving multienzyme cascades with incompatible reaction steps by compartmentalization, ACS Catal. 7 (2017) 3900–3904, https://doi.org/10.1021/acscatal.7b00776.
[16] C. Edlinger, T. Einfalt, M. Spulber, A. Car, W. Meier, C.G. Palivan, Biomimetic strategy to reversibly trigger functionality of catalytic Nanocompartments by the insertion of pH-responsive biovalves, Nano Lett. 17 (2017) 5790–5798, https://doi.org/10.1021/acs.nanolett.7b02886.
[17] J. Gaitzsch, D. Appelhans, L. Wang, G. Battaglia, B. Voit, Synthetic bio-nanoreactor: mechanical and chemical control of Polymersome membrane permeability, Angew. Chem. Int. Ed. 51 (2012) 4448–4451, https://doi.org/10.1002/anie.201108814.
[18] H. Yin, S.-W. Kang, Y.H. Bae, Polymersome formation from AB_2 type 3-Miktoarm star copolymers, Macromolecules 42 (2009) 7456–7464, https://doi.org/10.1021/ma901701w.
[19] T. Smart, H. Lomas, M. Massignani, M.V. Flores-Merino, L.R. Perez, G. Battaglia, Block copolymer nanostructures, Nano Today 3 (2008) 38–46, https://doi.org/10.1016/S1748-0132(08)70043-4.
[20] J. Lefley, C. Waldron, C.R. Becer, Macromolecular design and preparation of polymersomes, Polym. Chem. 11 (2020) 7124–7136, https://doi.org/10.1039/D0PY01247E.
[21] S. Lin, F. Wang, J. Du, High-genus multicompartment vesicles evolved from large compound micelles, Polym. Chem. 12 (2021) 3362–3366, https://doi.org/10.1039/D1PY00654A.
[22] Cameron, N. S.; Corbierre, M. K.; Eisenberg, A. 1998 E.W.R. Steacie award lecture Asymmetric amphiphilic block copolymers in solution: a morphological wonderland. *Can. J. Chem.* **1999**, *77*, 1311–1326. doi:https://doi.org/10.1139/v99-141.
[23] A.O. Moughton, T. Sagawa, L. Yin, T.P. Lodge, M.A. Hillmyer, Multicompartment micelles by aqueous self-assembly of μ-a(BC)n Miktobrush terpolymers, ACS Omega 1 (2016) 1027–1033, https://doi.org/10.1021/acsomega.6b00284.
[24] D. Ikkene, A.A. Arteni, C. Boulogne, J.-L. Six, K. Ferji, Multicompartment vesicles: a key intermediate structure in polymerization-induced self-assembly of graft copolymers, Macromolecules 55 (2022) 4268–4275, https://doi.org/10.1021/acs.macromol.2c00561.
[25] N. Ozawa, T. Nishimura, Macromolecular architectural effects on solution self-assembly of amphiphilic AB-type block copolymers, Polym. Chem. 15 (2024) 349–370, https://doi.org/10.1039/D3PY01324C.
[26] C. Booth, D. Attwood, Effects of block architecture and composition on the association properties of poly(oxyalkylene) copolymers in aqueous solution, Macromol. Rapid Commun. 21 (2000) 501–527, https://doi.org/10.1002/1521-3927(20000601)21:9%3C501::AID-MARC501%3E3.0.CO;2-R.
[27] L. Song, H. Sun, X. Chen, X. Han, H. Liu, From multi-responsive tri- and diblock copolymers to diblock-copolymer-decorated gold nanoparticles: the effect of architecture on micellization behaviors in aqueous solutions, Soft Matter 11 (2015) 4830–4839, https://doi.org/10.1039/C5SM00859J.
[28] S. Honda, T. Yamamoto, Y. Tezuka, Tuneable enhancement of the salt and thermal stability of polymeric micelles by cyclized amphiphiles, Nat. Commun. 4 (2013) 1574, https://doi.org/10.1038/ncomms2585.
[29] E.B. Zhulina, O.V. Borisov, Effect of block copolymer architecture on morphology of self-assembled aggregates in solution, ACS Macro Lett. 2 (2013) 292–295, https://doi.org/10.1021/mz400035k.
[30] X. Wang, C.A. Figg, X. Lv, Y. Yang, B.S. Sumerlin, Z. An, Star architecture promoting morphological transitions during polymerization-induced self-assembly, ACS Macro Lett. 6 (2017) 337–342, https://doi.org/10.1021/acsmacrolett.7b00099.
[31] N. Ozawa, J. Ha Lee, I. Akiba, T. Nishimura, Exploring the effects of glyco-copolymer architectures on the solution self-assembly of amphiphilic thermoresponsive linear, star, and cyclic polymers, Polym. Chem. 14 (2023) 3834–3842, https://doi.org/10.1039/D3PY00729D.
[32] A. Karatzas, J.S. Haataja, D. Skoulas, P. Bilalis, S. Varlas, P. Apostolidi, S. Sofianopoulou, E. Stratikos, N. Houbenov, O. Ikkala, H. Iatrou, Macromolecular architecture and encapsulation of the anticancer drug Everolimus control the self-assembly of amphiphilic polypeptide-containing hybrids, Biomacromolecules 20 (2019) 4546–4562, https://doi.org/10.1021/acs.biomac.9b01331.
[33] C. LoPresti, H. Lomas, M. Massignani, T. Smart, G. Battaglia, Polymersomes: nature inspired nanometer sized compartments, J. Mater. Chem. 19 (2009) 3576–3590, https://doi.org/10.1039/b818869f.
[34] G. Battaglia, A.J. Ryan, Bilayers and interdigitation in block copolymer vesicles, J. Am. Chem. Soc. 127 (2005) 8757–8764, https://doi.org/10.1021/ja050742y.
[35] F. Itel, A. Najer, C.G. Palivan, W. Meier, Dynamics of membrane proteins within synthetic polymer membranes with large hydrophobic mismatch, Nano Lett. 15 (2015) 3871–3878, https://doi.org/10.1021/acs.nanolett.5b00699.
[36] C. Effenberg, J. Gaitzsch, Stretched or wrinkled? Looking into the polymer conformation within polymersome membranes, Soft Matter 20 (2024) 4127–4135, https://doi.org/10.1039/D4SM00239C.
[37] F. Itel, M. Chami, A. Najer, S. Lörcher, D. Wu, I.A. Dinu, W. Meier, Molecular organization and dynamics in Polymersome membranes: a lateral diffusion study, Macromolecules 47 (2014) 7588–7596, https://doi.org/10.1021/ma5015403.
[38] B. van Bochove, S. Spoljaric, J. Seppälä, P. Sotta, A. Rios de Anda, Multiscale structural characterization of biocompatible poly(trimethylene carbonate) photoreticulated networks, ACS Appl. Polym. Mater. 1 (2019) 1811–1820, https://doi.org/10.1021/acsapm.9b00338.
[39] C. Hörtz, A. Birke, L. Kaps, S. Decker, E. Wächtersbach, K. Fischer, D. Schuppan, M. Barz, M. Schmidt, Cylindrical brush polymers with Polysarcosine side chains: a novel biocompatible carrier for biomedical applications, Macromolecules 48 (2015) 2074–2086, https://doi.org/10.1021/ma502497x.
[40] A.P. Pêgo, D.W. Grijpma, J. Feijen, Enhanced mechanical properties of 1,3-trimethylene carbonate polymers and networks, Polymer 44 (2003) 6495–6504, https://doi.org/10.1016/S0032-3861(03)00668-2.
[41] R. Xu, A. Dehghan, A.-C. Shi, J. Zhou, Elastic property of membranes self-assembled from diblock and triblock copolymers, Chem. Phys. Lipids 221 (2019) 83–92, https://doi.org/10.1016/j.chemphyslip.2019.03.015.
[42] W. Hao, Y.M. Chesnokov, V.S. Molchanov, P.R. Podlesnyi, A.I. Kuklin, V.V. Skoi, O. E. Philippova, Cryo-electron tomography study of the evolution of wormlike micelles to saturated networks and perforated vesicles, J. Colloid Interface Sci. 672 (2024) 431–445, https://doi.org/10.1016/j.jcis.2024.06.011.

[43] S. Jain, F.S. Bates, On the origins of morphological complexity in block copolymer surfactants, Science 300 (2003) 460–464, https://doi.org/10.1126/science.1082193.
[44] P.J. Schuetz, M. Greenall, J. Bent, S. Furzeland, D.F. Atkins, M.B. Butler, T.C. A. McLeish, D.M. Buzza, Controlling the micellar morphology of binary PEO–PCL block copolymers in water –THF through controlled blending, Soft Matter 7 (2011) 749–759, https://doi.org/10.1039/C0SM00938E.
[45] C.K. Haluska, W.T. Góźdź, H.-G. Döbereiner, S. Förster, G. Gompper, Giant hexagonal superstructures in Diblock-copolymer membranes, Phys. Rev. Lett. 89 (2002) 238302, https://doi.org/10.1103/PhysRevLett.89.238302.
[46] C. Lebleu, L. Rodrigues, J.-M. Guigner, A. Brûlet, E. Garanger, S. Lecommandoux, Self-assembly of PEG-b-PTMC copolymers: micelles and Polymersomes size control, Langmuir 35 (2019) 13364–13374, https://doi.org/10.1021/acs.langmuir.9b02264.
[47] W. Qi, P.P. Ghoroghchian, G. Li, D.A. Hammer, M.J. Therien, Aqueous self-assembly of poly(ethylene oxide)-block-poly(ε-caprolactone) (PEO-b-PCL) copolymers: disparate diblock copolymer compositions give rise to nano- and meso-scale bilayered vesicles, Nanoscale 5 (2013) 10908–10915, https://doi.org/10.1039/C3NR03250G.
[48] L. Zhang, A. Eisenberg, Multiple morphologies and characteristics of “crew-cut” micelle-like aggregates of polystyrene-b-poly(acrylic acid) Diblock copolymers in aqueous solutions, J. Am. Chem. Soc. 118 (1996) 3168–3181, https://doi.org/10.1021/ja953709s.
[49] P. Linse, Micellization of poly(ethylene oxide)-poly(propylene oxide) block copolymer in aqueous solution: effect of polymer impurities, Macromolecules 27 (1994) 2685–2693, https://doi.org/10.1021/ma00088a006.
[50] H. Bermudez, A.K. Brannan, D.A. Hammer, F.S. Bates, D.E. Discher, Molecular weight dependence of Polymersome membrane structure, elasticity, and stability, Macromolecules 35 (2002) 8203–8208, https://doi.org/10.1021/ma020669l.
[51] M.W. Matsen, F.S. Bates, Testing the strong-stretching assumption in a block copolymer microstructure, Macromolecules 28 (1995) 8884–8886, https://doi.org/10.1021/ma00130a029.
[52] J.-F. Le Meins, O. Sandre, S. Lecommandoux, Recent trends in the tuning of polymersomes’ membrane properties, Eur. Phys. J. E: Soft Matter Biol. Phys. 34 (2011) 14, https://doi.org/10.1140/epje/i2011-11014-y.